IOPscience iopscience.iop.org

Home Search Collections Journals About Contact us My IOPscience

Fabrication and analysis of high-performance piezoelectric MEMS generators

This content has been downloaded from IOPscience. Please scroll down to see the full text.

2012 J. Micromech. Microeng. 22 065017

(http://iopscience.iop.org/0960-1317/22/6/065017)

View the table of contents for this issue, or go to the journal homepage for more

Download details:

IP Address: 130.133.8.114
This content was downloaded on 22/05/2017 at 07:56

Please note that terms and conditions apply.

You may also be interested in:

Piezoelectric MEMS generators fabricated with an aerosol deposition PZT thin film
B S Lee, S C Lin, W J Wu et al.

The design, fabrication and evaluation of a MEMS PZT cantilever
Dongna Shen, Jung-Hyun Park, Jyoti Ajitsaria et al.

Piezoelectric micro energy harvesters based on stainless-steel substrates
Shun-Chiu Lin and Wen-Jong Wu

Fabrication of PZT MEMS energy harvester based on silicon and stainless-steel substrates utilizing an aerosol deposition method
Shun-Chiu Lin and Wen-Jong Wu

Fabrication and performance evaluation of a metal-based bimorph piezoelectric MEMS generator for vibration energy harvesting
Chun-Liang Kuo, Shun-Chiu Lin and Wen-Jong Wu

Corrugated aluminum nitride energy harvesters for high energy conversion effectiveness
Ting-Ta Yen, Taku Hirasawa, Paul K Wright et al.

Fabrication and characterization of MEMS-based PZT/PZT bimorph thick film vibration energy harvesters
R Xu, A Lei, C Dahl-Petersen et al.

Preparation of a high-quality PZT thick film with performance comparable to those of bulk materials
Xiao-Hui Xu and Jia-Ru Chu

J. Micromech. Microeng. **22** (2012) 065017 (9pp) doi:10.1088/0960-1317/22/6/065017

Fabrication and analysis of high-performance piezoelectric MEMS generators

Gang Tang[1,2], Jing-quan Liu[1], Bin Yang[1], Jiang-bo Luo[1], He-sheng Liu[3], Yi-gui Li[1], Chun-sheng Yang[1], Dan-nong He[4], Viet Dzung Dao[5], Katsuhiko Tanaka[5] and Susumu Sugiyama[5]

[1] National Key Laboratory of Science and Technology on Nano/Micro Fabrication/Institute of Micro and Nano Science and Technology, Shanghai Jiaotong University, Shanghai 200240, People's Republic of China
[2] Department of Mechanical and Engineering, Nanchang Institute of Technology, Nanchang 330099, People's Republic of China
[3] School of Physics and Electronic Information, Shangrao Normal University, Shangrao 334001, People's Republic of China
[4] National Engineering Research Center for Nanotechnology, Shanghai 200241, People's Republic of China
[5] Department of Micro System Technology, Ritsumeikan University, 1-1-1 Noji-Higashi, Kusatsu, Shiga, Japan

E-mail: jqliu@sjtu.edu.cn

Received 30 January 2012, in final form 26 March 2012
Published 17 May 2012
Online at stacks.iop.org/JMM/22/065017

Abstract
In this paper, we have designed a fabrication process for microgenerators by bonding a piezoelectric ceramic $Pb(Zr,Ti)O_3$ (PZT) plate to a silicon on insulator (SOI) wafer. The key techniques of the process include the low-temperature bonding technique using conductive epoxy resin, thinning of the bulk PZT using mechanical lapping and wet-etching combined method, and the micromachining of bulk ceramics by dicing. Through the development and optimization of the process, a piezoelectric MEMS power generator array was successfully fabricated. The typical device is selected to characterize the output performance of the microgenerators, while the composite beam dimension of PZT and silicon layer is about 3080 μm $\times$ 800 μm $\times$ 31 μm and the dimension of Ni proof mass is about 900 μm $\times$ 800 μm $\times$ 450 μm. The experimental results show that the output voltage, output power and power density of this device are 2.72 $V_{P\text{-}P}$, 11.56 μW and 28 856.7 μW cm^{-3} at the resonant frequency of 514.1 Hz when it matches an optimal resistive load of 70 kΩ under the excitation of 1g acceleration. The output performance of this device is higher, compared with that of other reported MEMS power generators, which demonstrates that this novel technique has great potential to fabricate high-performance piezoelectric MEMS energy harvester.

(Some figures may appear in colour only in the online journal)

1. Introduction

The rapidly decreasing size, cost and power consumption of sensors and electronics devices have opened up the relatively new research field of energy harvesting [1]. A lot of research has been done on energy harvesting from external mechanical excitation, specifically focused on developing piezoelectric energy-harvesting devices by MEMS technology [1–13, 16]. Because piezoelectric converters have simple structure, high electromechanical coupling coefficient, no requirement of external voltage source and long lifetime, they are quite attractive for the application of volume-limited

 © 2012 IOP Publishing Ltd Printed in the UK & the USA

wireless sensor node [7]. The piezoelectric coefficients of piezoelectric materials would affect the output performance of the generator. Marzencki *et al* [8] reported a cantilever generator with a thin film AlN deposited by the sputtering process, which can generate 1.97 μW from 4g acceleration at its resonant frequency of 1368 Hz. Yen *et al* [9] developed aluminum nitride energy harvesters with corrugated cantilever structures which can have an energy conversion effectiveness comparable to a conventional bimorph design. Under an input acceleration of 0.25g, the amplitude of the output voltage was 92 mV at a load resistance of 0.86 MΩ and the calculated output power is 4.9 nW. In order to obtain higher output power, a multifold corrugated cantilever was designed and the output power of 0.17 μW can be obtained under acceleration of 1g at its resonant frequency of 853 Hz. The output power of the above-fabricated devices is limited to low power levels by the low piezoelectric properties of AlN. Generally, PZT (piezoelectric ceramic lead zirconate titanate) is a practical material for microgenerators because of its excellent piezoelectric properties and most piezoelectric MEMS generators are formed using PZT materials together with silicon substrate. Fang *et al* [10] demonstrated a MEMS-based PZT cantilever power generator with a nonintegrated Ni proof mass, which generated the power of 2.16 μW at 608 Hz resonant frequency. Shen *et al* [11] successfully fabricated a MEMS-based PZT cantilever microgenerator with an integrated proof mass that can generate 2.15 μW from 2g acceleration at its resonant frequency of 416.5 Hz. Jeon *et al* [12] designed a thin film PZT microgenerator operated under d_{33} mode, which was realized by interdigitated electrodes. For all these structures mentioned above, the thin PZT film layer was deposited by the sol-gel process, and its corresponding thickness was restricted to less than 2 μm. Thus it resulted in a low-output voltage and power. To obtain a sufficiently powerful energy harvester, it is however desirable to use thicker PZT films [13]. Lee *et al* [14] developed two types of piezoelectric MEMS generators with thick film PZT, i.e. d_{31} mode and d_{33} mode. For these two piezoelectric MEMS generators, the PZT film of thickness 5 μm was prepared by using an aerosol deposition method. The fabricated 31 mode device possesses a maximum output power of 2.765 μW at a resonant frequency of 255.9 Hz under a 2.5g acceleration level. A PZT thick film fabricated by the screen-printing technique was reported for a vibration energy harvester with 14.0 μW at 1g input acceleration. The thick films formed by using the techniques mentioned above, whether screen-printing or aerosol deposition, are not dense due to the restriction of the sintering temperature [15], and some properties such as piezoelectricity and dielectric constant are poor compared with those of bulk PZT ceramics. Such films are not suitable for microgenerators that require large output performance.

In recent years, a useful technique for preparing PZT thick films on silicon has been investigated, which is the wafer bonding of bulk PZT and silicon using an intermediate layer and then thinning PZT [15–18]. There is no doubt that high-performance bulk PZT may significantly improve the performance of piezoelectric microgenerators. Tanaka *et al* [15] prepared PZT thick films by adopting the bonding technology using Au as the intermediate layer and mechanical lapping method. However, the bonding process needs special fabrication processing and bonding equipment, thus costs are high. At the same time, because the bonding temperature was higher than 500 °C, some problems would appear, such as repolarization issue and the larger residual stress caused by the thermal mismatch between the PZT ceramics and silicon substrate. Recently, Aktakka *et al* [16] reported a thinned-PZT/Si unimorph for vibration energy harvesting. The harvester utilizes thinning of bulk-PZT pieces bonded to an SOI wafer. Au/In of thickness 5 μm was used as the bonding layer and the bonded bulk PZT was thinned to the thickness of about 20 μm by the mechanical lapping method. In order to reduce fabrication cost of the intermediate layer of Au, epoxy resins as an intermediate layer and wet-etching process for thinning down PZT thickness were demonstrated [17]. Because the used epoxy resins were nonconductive, it was very difficult to expose the bottom electrodes for output signal by the micromachining process. Wang *et al* [18] developed the integration of bulk PZT and silicon by Cytop, a patternable bond layer, and the thinning of the bulk PZT by the chemical mechanical polishing method.

In this paper, a novel process to fabricate low-frequency vibration piezoelectric MEMS generators is proposed by bonding bulk PZT on an SOI structure. The key techniques for fabricating microgenerators are described, including the bulk PZT-Si bonding and bulk PZT thinning and patterning. Conductive epoxy resins are used as the intermediate adhesive and conductive layer. Mechanical lapping and wet-etching combined method are proposed for bulk PZT thinning and the dicing technique is used as the bulk PZT patterning process. A unimorph PZT cantilever constructed with an Au/Cr/PZT/conductive epoxy/Cr/Au/SiO_2/Si/SiO_2 multilayer structure with micromachined Ni proof mass was designed and fabricated. Finally, the output performance of the fabricated device with typical dimension was tested and evaluated.

2. Basic design of the fabrication process and key techniques

A cantilever beam structure is commonly used in piezoelectric microgenerators. The basic fabrication process for a cantilever beam structure is outlined in figure 1. Firstly, the surfaces of bulk PZT and silicon wafers are polished. Then, the two wafers are bonded together. Following that, the bulk PZT wafer is thinned to a suitable thickness and the thinned PZT wafer is micromachined into the desired pattern by the dicing method. Finally, the back surface of the silicon wafer is structured with a wet or dry etching process.

2.1. Wafer bonding and bulk PZT thinning

One of the key techniques in the above process is bonding the bulk PZT wafer to the silicon wafer. A realizable and repeatable bonding process requires that it does not alter the properties and performance of the components during

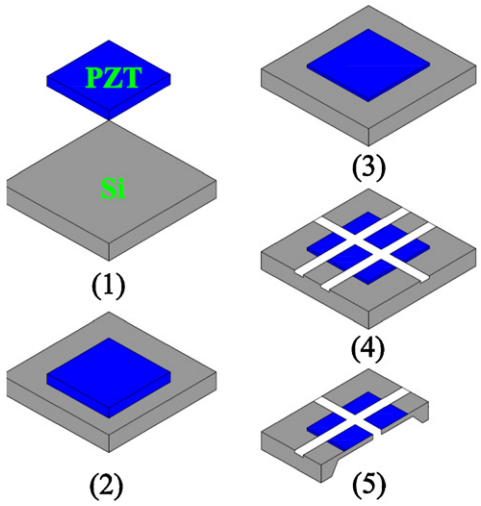

Figure 1. Basic fabrication process of cantilever beam structures for microgenerators using bulk PZT.

bonding. Hence, several bonding conditions must be satisfied to ensure the precision of the cantilever beam structure. Firstly, a low-temperature bonding process is essential to reduce the detrimental effect of thermal mismatch between the PZT ceramics and silicon and be compatible with subsequent processes. Secondly, the thickness of the intermediate bonding layer should be less than several microns. Thirdly, the thickness uniformity of the intermediate bonding layer should be controlled well in order to thin down bulk PZT and obtain its uniformity. Fourthly, the intermediate bonding layer should be conductive. Otherwise, the bottom electrodes will be very difficult to expose. Finally, the bonding strength should be high enough to obtain good reliability of the fabricated device, and remain stable under about 150 °C operating temperature needed in later MEMS processes.

To satisfy these conditions, a conductive epoxy organic adhesive material as an intermediate bonding layer is deployed to bond bulk PZT and silicon wafers at temperatures as low as 175 °C. The conductive epoxy resins (DAD-91L, Shanghai Research Institute of Synthetic Resins) used in the bonding experiments feature high bonding strength and the typical bond strength is more than 8 MPa. Moreover, the material has a high continuous operating temperature of about 250 °C. Good adhesion and thermoplastic characteristics of this material make it an appropriate intermediate layer for low-temperature bonding. One or two layers of conductive epoxy resin were firstly screen printed on the silicon wafer. Then, the PZT and silicon wafer were bonded together face to face under a specified pressure and heated at suitable gradient temperatures in an vacuum oven which are from 60 °C up to 175 °C according to 15 °C per 10 min and holding for more than 1 h at 175 °C. The gradient temperatures and the vacuum oven are necessary to obtain a uniform epoxy layer and remove air bubbles from the bonding layer. The pressure was removed when the temperature reached room temperature.

The bonding strength of the PZT–conductive epoxy-Si wafers can be measured by the conventional tensile test [19] using a microtensile tester (Instron Model 5868). Figure 2 shows the experimental set-up for the bonding strength test.

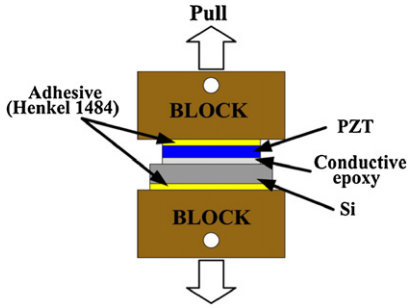

Figure 2. A schematic diagram of the experimental set-up for bonding strength measurement.

The bonded chips were fixed to the clamping apparatus using a glue epoxy (Henkel 1484) layer. The bond strength of the glue is more than 30 MPa. Then, the clamp was pulled apart under a certain pull force and speed. Controlling software is available to record the tensile and strain data. The applied bonding pressure was shown to be an important bonding parameter.

The other key technique in this fabrication process is the thinning of bulk PZT. Generally, it is difficult to thin down the ceramic plate to less than 50 μm due to its brittleness. However, bulk PZT with a thickness of about 10 μm or less can be obtained by wet-etching or lapping PZT after bonding it to the silicon wafer [15–18]. The etching rate of bulk PZT by the wet-etching method is low and the thickness uniformity of bulk PZT is very difficult to control by mechanical lapping machine when its thickness is lower than 30 μm. Therefore, the hybrid method of mechanical lapping and wet-etching processes is deployed to thin down the bulk PZT. Several hundred microns thickness PZT was thinned down to about 30 μm by using mechanical lapping. Then, a wet-etching process was used for PZT ceramics thinning down to the required thickness using 1BHF:2HCl:4NH_4Cl:4H_2O as the etchant [17]. Finally, an additional mechanical polishing process on the PZT films was applied to improve the surface roughness of PZT for subsequent fabrication processes [17].

2.2. Patterning of bulk PZT

Patterning and micromachining PZT bulk ceramics is very important for microgenerators using bulk PZT. Some methods had been reported to pattern and micromachine PZT, for example, dicing, reactive ion etching (RIE), wet etching or KrF excimer laser. It is known that the etching rate of PZT is very slow through the RIE method, whereas accuracy of pattern is difficult to obtain using wet etching or a KrF excimer laser. Dicing is a low-cost method for micromachining PZT wafers and can achieve a comparatively accurate pattern.

A commercially available ADT7100 dicing machine is used to pattern the bulk PZT. The micromachining precision of this dicing machine is 0.1 μm, which can ensure the uniformity of cutting bulk PZT. The cutting velocity and the spindle speed are 6 mm s^{-1} and 14 000 n min^{-1}, respectively.

Figure 3 shows a SEM image of a PZT rectangular pole array that was obtained by dicing a PZT wafer with a 60 μm thick blade. The pole pitch was about 120 μm. It is demonstrated that the desirable shape size in straight lines could be accurately obtained.

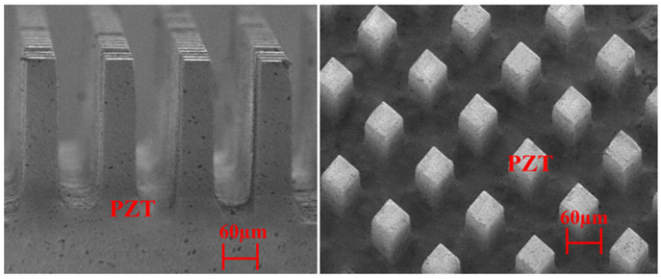

Figure 3. SEM images of the PZT rectangular pole array made by dicing. (*a*) Cross-sectional view, (*b*) front side 45° view.

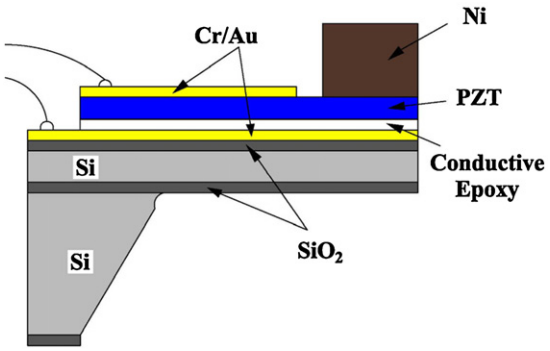

Figure 4. Layer sequence of the piezoelectric micropower generator.

3. Fabrication and measurement of piezoelectric microgenerators

For the purpose of converting vibration energy into electric power, a composite cantilever beam structure with optional proof mass was adopted, as shown in figure 4. The whole structure was based on a SOI wafer. The metal mass on the free end of the cantilever is used to amplify ambient vibrations, decreasing the structure's natural frequency. The composite cantilever is made up of the top electrode (Au/Cr), PZT thick film, conductive epoxy, the bottom electrode (Au/Cr) and with a lower nonpiezoelectric element. The electrodes are used to exploit the 31 excitation mode of the PZT material which may have a greater advantage in MEMS applications [20, 24, 25]. Generally, for practical applications, the targeted application environment, that is, the vibration frequency and the acceleration amplitude, should be known. To obtain the maximum power output, the cantilevered beam device should be designed to resonate at a specific frequency of the vibration of the structure where the device is mounted. The natural frequency of the power generator can be regulated to match the fundamental frequency of its environment by varying the structured dimensions of the proof mass.

3.1. Fabrication

The prototype device was fabricated using silicon-on-insulator (SOI) micromachining technology because the thickness of the supported Si cantilever is easy to control. The SOI wafer used has a 10 μm thick heavily doped silicon device layer, 2 μm thick buried oxide (BOX) layer and a 450 $\pm$ 20 μm thick

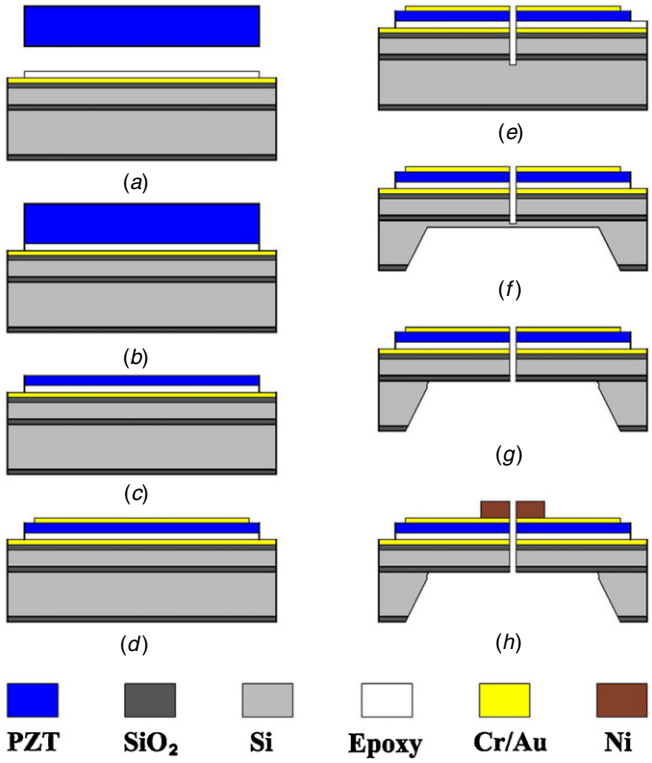

Figure 5. Fabrication process of microgenerator. (*a*) Bottom electrode deposition and screen printing of conductive epoxy resins on the SOI wafer, (*b*) bonding PZT and SOI wafers, (*c*) thinning down the PZT layer by using the mechanical lapping and wet-etching combined method, (*d*) top electrode deposition and pattern, (*e*) bulk PZT micromachining by the dicing method, (*f*) back oxide window creation by HF solution etching and silicon deep etching by a KOH solution, (*g*) cantilever release by the XeF_2 etching system and (*h*) metal mass microfabrication and assemblage.

substrate. 2 μm thick silicon oxide was grown on both sides of the SOI wafer by a wet O_2 method, which was used as electrical isolation layer and hard mask during silicon wet etching. A 50/150 nm Cr/Au layer as a bottom electrode was deposited by magnetron sputtering and one layer of conductive epoxy resin was screen printed, as shown in figure 5(*a*). Then, the PZT and the prepared silicon wafer were bonded together facing each other (figure 5(*b*)). Figure 5(*c*) shows that the PZT layer was thinned down to the thickness needed. The Cr/Au layer as the top electrode was sputtered and patterned on the PZT layer (figure 5(*d*)). Then, the bulk PZT was micromachined and patterned by the dicing method and the depth of cutting should be under the buried oxide layer, as shown in figure 5(*e*). Similar processes have been demonstrated in our previous work [23], as shown in figures 5(*f*)–(*h*). An Au/Cr/PZT/conductive-epoxy/Cr/Au/SiO_2/Si/SiO_2 multilayer cantilever structure with a nickel mass was successfully fabricated.

3.2. Experimental results and discussion

For the above-microfabricated generator, the effect of bonding pressure on the bonding strength has been investigated. A total of 6 mm $\times$ 6 mm bonding specimens were prepared and measured. Figure 6 shows the bonding strengths of the

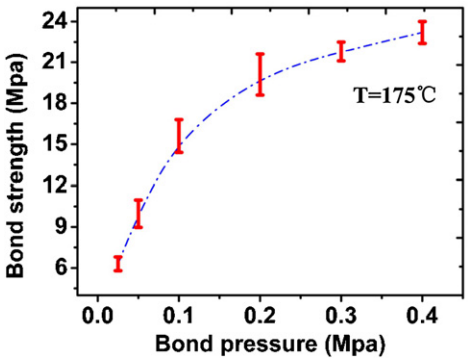

Figure 6. Realized bond strength depending on the bond pressure at the curing temperature of 175 °C.

PZT–conductive epoxy–Si-bonded wafers as a function of applied pressure at the curing temperature of 175 °C during bonding. It can be seen that the bonding strength was more than 10 MPa at an applied pressure of 0.1 MPa. Increasing the bond pressure contributed to improving the bond strength, which resulted from the decrease in the number of voids. But the bonded wafers could be easily deformed or damaged under higher bond pressure. Therefore, the applied pressure of 0.1 MPa during bonding would be a relatively ideal value for its application. In addition, the error bar in figure 6 shows multiexperimental results and obtains good uniformity of bonding strength.

For the application of microgenerators, the open circuit voltage can be expressed as [12]

$$V = \sigma_{xx} g_{31} H \tag{1}$$

where σ_{xx} is the stress in the x-direction, H is the thickness of the piezoelectric material and g_{31} is the piezoelectric coefficient, so the increased thickness of the PZT layer can contribute to improve the power output. However, the natural frequency of the designed structure is approximately given as

$$\omega = \sqrt{k/m} \tag{2}$$

where k is its stiffness and m is the mass. It indicates that the natural frequency is proportional to the stiffness, i.e. the thickness of the PZT layer. Thus, to obtain higher power output under lower natural frequency of the available ambient source, the thickness of the PZT layer is determined to be 10–20 μm.

The minimum thickness of thinned PZT can be controlled and remained at about 14 μm, as shown in figure 7. The thickness of the epoxy bonding layer is about 3.3 μm.

The properties of 15 μm bulk PZT after thinning were tested in our previous work [23]. It shows that the dielectric loss is in the range of 1.7–3%, which is normal for most PZT ceramics [17].

Based on the optimization bonding and thinning process, a piezoelectric microgenerator array was fabricated, which included cantilevers with different lengths and widths and Ni-proof masses with different dimensions assembled on their tips, as shown in figure 8. The gap between adjacent beams was about 100 μm, which can be ensured by the thickness of the blade in dicing.

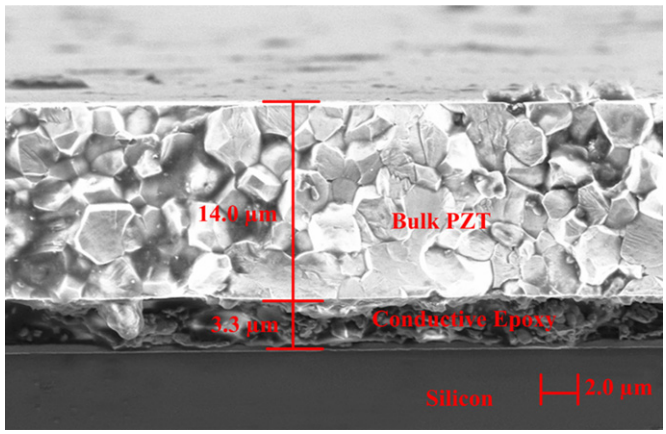

Figure 7. SEM image of cross-section of the PZT-Si-bonded wafer.

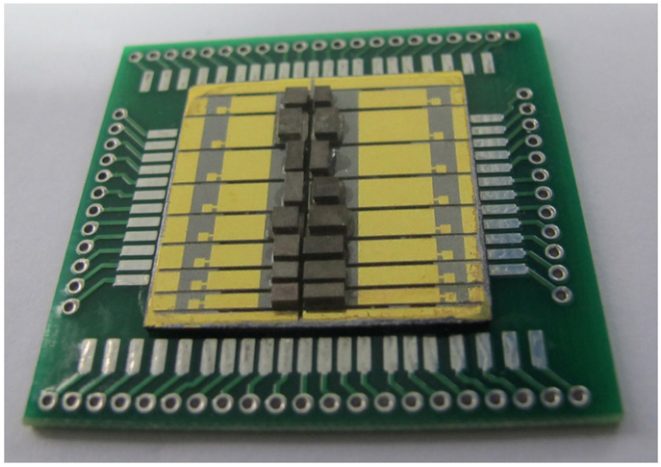

Figure 8. Microfabricated piezoelectric cantilever devices assembled with PCB.

Figure 9 shows SEM images of a typical device. From figure 9(*a*) we can see the clearly straight cantilever beam along with the Ni-proof mass. It demonstrates the practicable layer structure of the device and the fabrication process. The straight beam slightly bending shows the residual stress in the PZT film, which results from the mismatch of the thermal expansion coefficients of Si and PZT. Fortunately, the thermal expansion coefficients of PZT is almost the same as that of single crystal silicon in the temperature range from 25 °C to 175 °C [15]. Therefore, the thermal mismatch stress at the bonding interface is very small, which ensures smaller distortion of the fabricated cantilever. Figure 9(*b*) shows the cross-sectional view with the high-quality bonding interface after thinning down the PZT. The well-developed grain structure of the bulk PZT is also clearly seen, which is dense and guarantees excellent piezoelectricity and cannot be attained by the conventional methods of PZT films. The thickness of the PZT layer after thinning and the Si substrate after KOH and XeF_2 etching are uniform throughout the diaphragm. The latter is ensured by the SOI wafer, which will highly decrease the difference between the designed and the experimental resonant frequencies of the device.

The designed and measured dimensions of the typical device are listed in table 1. The measured dimensions and

Table 1. Dimensions and frequency of the typical device.

	Cantilever beam (μm) (length (l) × width (w) × thickness (t))					Ni mass (μm) (length (l) × width (w) × thickness (t))			
	l	w	t_{pzt}	t_{Si/SiO_2}	t_{epoxy}	l	w	t	Frequency (Hz)
Designed	3200	800	14.0	14.0	4.0	900	800	450	527.1 (simulated)
Measured	3080	800	14.2	13.5	3.4	900	800	450	519.0 (measured)

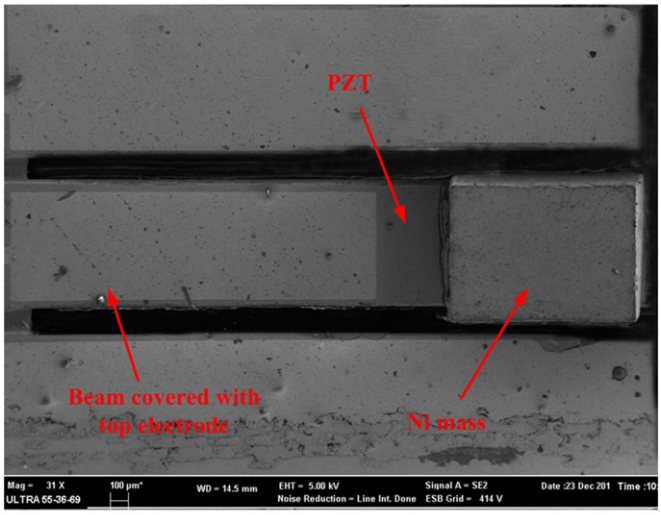

(*a*)

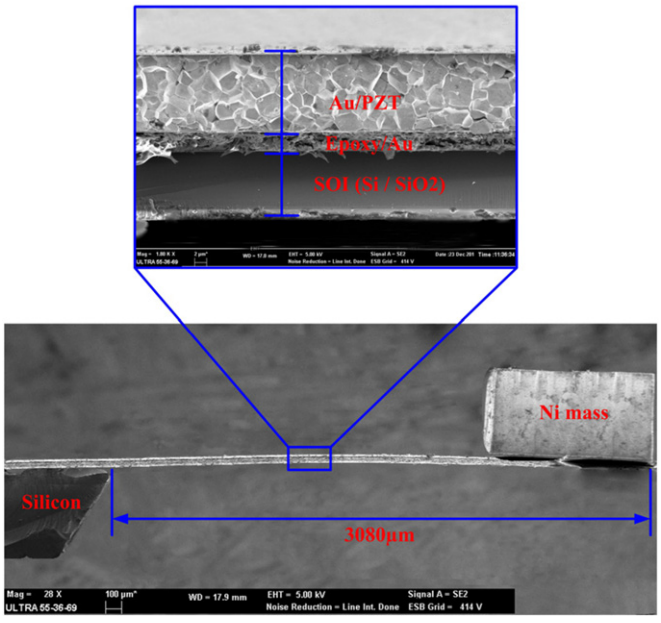

(*b*)

Figure 9. SEM images of a fabricated device with typical dimensions. (*a*) Front view, (*b*) cross-sectional view.

calculated volumes of the typical device are listed in table 1. The measured width of the cantilever beam and the thicknesses of the PZT layer and the supporting SiO_2/Si layer were exactly consistent with the designed dimensions, but the length of the cantilever beam was inconsistent with the design due to the difficulty in accurately controling silicon etching by the KOH wet and XeF_2 dry etching. However, DRIE is a good choice to precisely control the length of the beam in silicon etching.

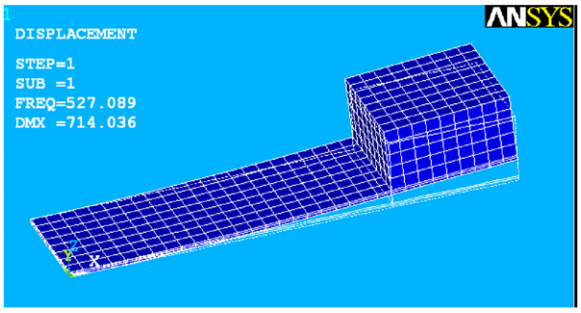

Figure 10. The simulation figure of the designed device for the first mode using ANSYS.

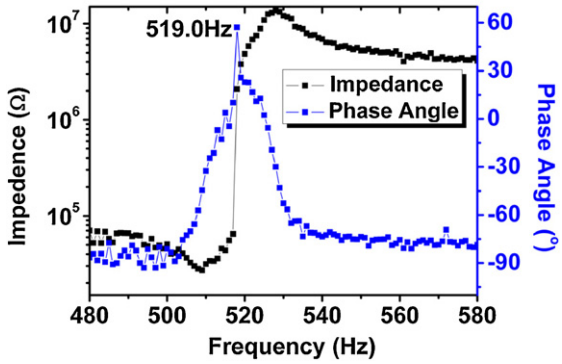

Figure 11. Measured resonant frequency of a typical device using the impedance analyzer.

The designed resonant frequency simulated by ANSYS, a multiphysics FEA tool, is about 527.1 Hz. The first resonant mode and its frequency are shown in figure 10. Figure 11 shows the measured phase angle of the typical device versus the exciting frequency using an impedance analyzer (HP E4194A). The peak of the phase–angle curve is at about 519.0 Hz. There is good agreement between theoretical and experimental results.

The output performance of the prototype was evaluated by a vibration testing system described previously [10]. It consists of an electromagnetic shaker (SINOCERA JZK-5), a power amplifier (SINOCERA YE2706A), a function waveform generator (Agilent 33220A), an accelerator (SINOCERA YE5932A). The piezoelectric device and the accelerometer were assembled onto the shaker. The vibration frequency and amplitude of the shaker were controlled by the function generator and the power amplifier, and the given vibration condition was monitored by the accelerometer. The output signal of the piezoelectric MEMS generator was connected to a different resistive load to obtain the relationship between load impedance and output behavior such as output power

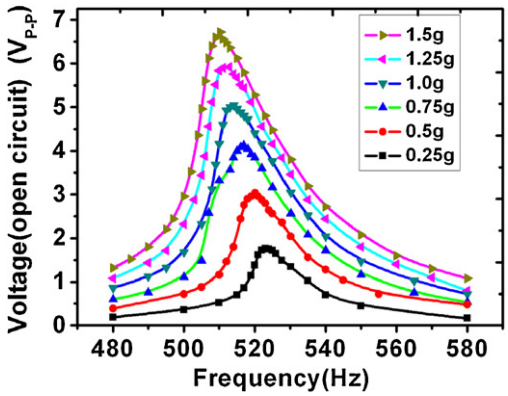

Figure 12. The peak–peak voltage under open circuit condition versus exciting vibration frequency at different vibration accelerations.

and output voltage at different vibration conditions. The voltage signals from the testing sample were monitored by the oscillograph (TEKtronix TDS2012B) and the corresponding output average powers were calculated by the following equation:

$$P = \left[\frac{U_{\text{Peak-Peak}}}{2}\Big/\sqrt{2}\right]^2\Big/R \tag{3}$$

where $U_{\text{Peak-Peak}}$ is the load voltage of ac peak–peak value, and R is the load resistance.

The peak–peak voltage under open circuit condition versus exciting vibration frequency was measured at different vibration levels (figure 12). It can be seen that the resonance frequencies of the device at 0.25g, 0.5g, 0.75g, 1.0g, 1.25g and 1.5g acceleration are 523.1 Hz, 520.1 Hz, 516.9 Hz, 514.1 Hz, 512.8 Hz and 510.3 Hz, respectively, which gradually decrease with the increase of the acceleration amplitude. The difference is mainly due to the nonlinear change in Young's modulus of PZT [16, 21]. In addition, the maximum peak–peak voltage under open circuit condition increases with increasing vibration acceleration value. However, the experimental results show that there exists a nonlinear relationship between the voltage and the acceleration amplitude. The voltage increased 72.7% from 1.76 V to 3.04 V when the vibration acceleration value increased from 0.25g to 0.5g, while it increased only 13.5% from 5.92 V to 6.72 V when the vibration acceleration value increased from 1.25g to 1.5g. This is because of the nonlinear response of PZT and the piezoelectric constant decreases with increasing stress when the acceleration amplitude increases [11, 16, 22].

When the resonant vibration was achieved, the output power of the generator was highly dependent on the load impedance and the maximum output power can be obtained under certain load impedance. Figure 13(a) shows the output voltage at different load impedances under different excited accelerations from 0.25g to 1.5g. Under a certain acceleration exciting condition, the output voltage increased with increasing loading impedance. The increasing trend at the range of lower matching impedance is larger than that under the condition of higher impedance.

Based on equation (3), the corresponding output power is shown in figure 13(b). With the increase of loading

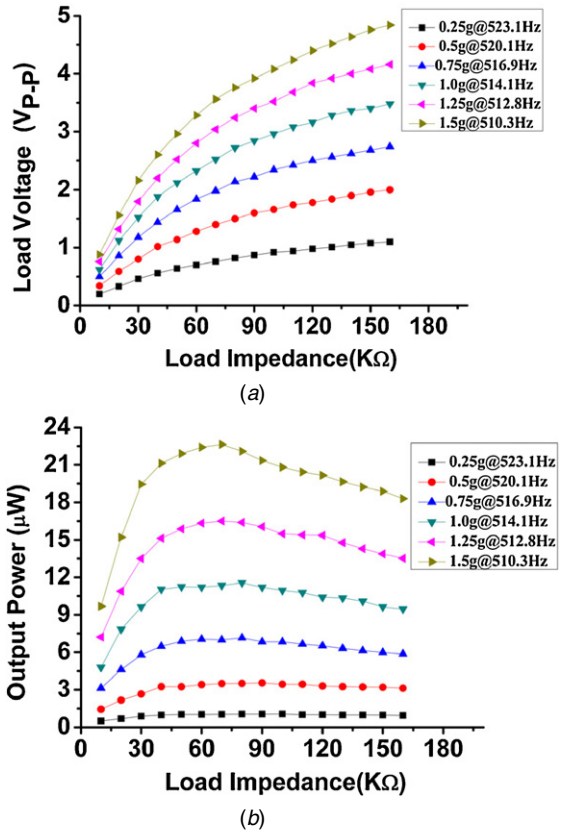

Figure 13. Load voltage and power delivered to the load versus resistance at different accelerations.

impedance, we found that the output power firstly increased and then decreased when at a certain acceleration. There is a peak value of output power under each excited acceleration condition at a certain resistive load, which is named the optimal-matched resistance. Meanwhile, we found that the optimal resistive load was dependent on the applied acceleration. With the increase of the vibration level, the optimal resistive load decreased gradually from 100 kΩ under 0.25g acceleration condition to 70 kΩ under 1.5g acceleration condition. This is due to an increase in the PZT dielectric constant and dielectric losses, both related to the high mechanical strain and high electric field in the material [16].

As shown in figure 13, at a 1g vibration, we found that the output power of the typical device had a peak value of 11.56 μW when the load resistance was 70 kΩ. At this maximum power output condition, the output voltage was 2.72 $V_{P\text{-}P}$, which was higher than the minimum requirement for the rectifier circuit diode band gaps [14].

In order to compare the output performance of the fabricated generator with different methods, the power density is deployed to evaluate it. Thus, the volume of our typical device is calculated as 0.4006 mm^3 and the power density of piezoelectric mechanisms is derived as 28 856.7 $\mu W\ cm^{-3}$. The fabrication methods of PZT film, the working conditions and power density of other published piezoelectric energy harvesters are listed in table 2 for comparison. This indicates that the power density of the piezoelectric device reported in this paper demonstrates comparable performance.

Table 2. Performance comparison among published piezoelectric harvesters and our device.

Author	Piezoelectric material	Input vibration (g)	Frequency (Hz)	Power output (μW)	Effective volume (mm^3)	Power density (μW cm^{-3})
Shen *et al* [5]	Sol–gel PZT	0.75	183.8	0.32	0.769	416
Marzencki *et al* [8]	Sputtered AlN	4.0	1368	1.97	>0.552[b]	<3569[b]
Yen *et al* [9]	Sputtered AlN	1.0	853	0.17	0.8205[b]	207[b]
Fang *et al* [10]	Sol–gel PZT	1.0	608	2.16	0.196[b]	11 020[b]
Shen *et al* [11]	Sol–gel PZT	2.0	462.5	2.15	0.6520	3272
Lei *et al* [13]	Screen printed PZT	1.0	235	14.0	12.888[b]	1086[b]
Lee *et al* [14]	Aerosol PZT	1.0	255.9	1.125	0.425[b]	2647[b]
Aktakka *et al* [16]	Thinned bulk PZT	1.5	154	205	17.955[b]	11 417[b]
Tang *et al* (this work)	Thinned bulk PZT	1.0	514.1	11.56	0.4006	28 856.7

[a] The effective volume is the sum of the volume of the cantilever beam and the volume of the proof mass.
[b] Estimated from data in reference.

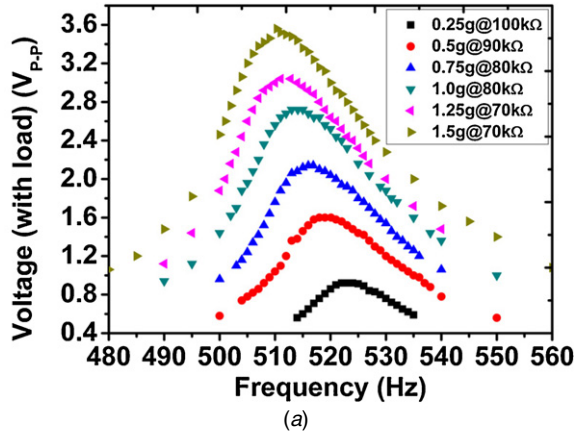

(*a*)

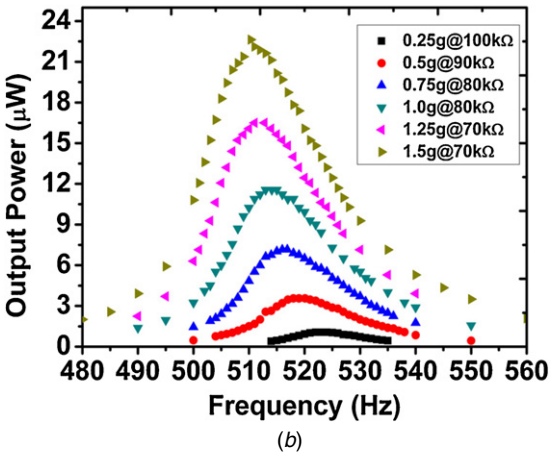

(*b*)

Figure 14. (*a*) Output voltage (*b*) and power with the optimal resistive load as a function of the input frequency for different input accelerations.

The output voltage and dissipated power in the optimal resistance load as a function of the frequencies near resonance for different accelerations are shown in figure 14. There is a peak value of the output voltage and power under each excited acceleration condition at the matching impedance. The peak shifts toward a lower frequency when the excitation acceleration increases, as mentioned above.

It is known that the quality factor of the device is related to sharpness of the plot. Figure 14 shows that the quality factor decreases with increasing acceleration. The decrease in quality

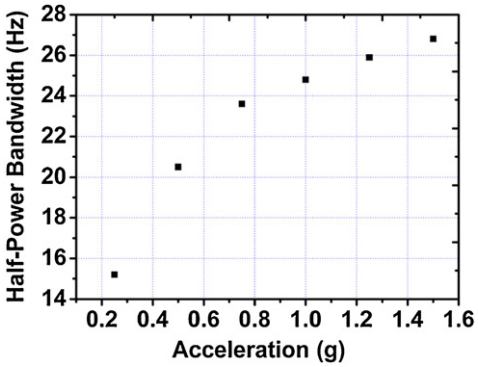

Figure 15. Bandwidth measured as a function of input acceleration.

factor is due to the electrical and structural damping increases at higher vibration levels and will increase the bandwidth of the resonant peaks [13, 16], as confirmed in figure 15. The bandwidth in figure 15 can be obtained directly from the measurements shown in figure 14(*b*). As seen, at 1*g* vibration, the determined half-power bandwidth of the device is about 25.9 Hz.

4. Conclusions

A novel process to fabricate cantilever microgenerators with bulk PZT was proposed. The advantage of using wafer bonding technology in piezoelectric MEMS generators is that we can directly utilize the excellent properties of bulk PZT. Bulk PZT could be applied to microgenerators by thinning and micromachining after being bonded to Si wafers. The fabricated typical device has beam dimensions of about 3080 μm $\times$ 800 μm $\times$ 31 μm with a Ni proof mass with dimensions of about 900 μm $\times$ 800 μm $\times$ 450 μm. The experimental results show that the device had a maximum output power of 11.56 μW with a 2.72 V_{P-P} output voltage at a resonant frequency of 514.1 Hz and a half-power bandwidth of 25.9 Hz at a 1*g* acceleration level when it matches an optimal resistive load of 70 kΩ. The power density is calculated as 28 856.7 μW cm^{-3}, which is superior to the devices fabricated by other technologies in the reported literature. The results show that the new process can be compatible with MEMS technology and the PZT thick film retains the excellent

performance of bulk PZT. This method provides a new way for the preparation of high-performance piezoelectric MEMS energy harvester.

Acknowledgments

The authors would like to acknowledge the financial support for this research from International Corporation Program of Ministry of Science and Technology of China (no 2009DFB10330), the National Natural Science Foundation of China (no 51035005), the External Corporation Program of Jiangxi Provincial Department of Science and Technology of China (no 2010EHAO2500), the Youth Science Fund of Jiangxi province office of education of China (no GJJ11248). The authors are also grateful to colleagues for their essential contribution to this work.

References

[1] Roundy S 2005 On the effectiveness of vibration-based energy harvesting *J. Intell. Mater. Syst. Struct.* **16** 809–23
[2] Aktakka E E, Kim H and Najafi K 2011 Energy scavenging from insect flight *J. Micromech. Microeng.* **21** 095016
[3] Elfrink R, Kamel T M, Goedbloed M, Matova S, Hohlfeld D, Andel Y V and Schaijk R V 2009 Vibration energy harvesting with aluminum nitride-based piezoelectric devices *J. Micromech. Microeng.* **19** 094005
[4] Liu H, Tay C J, Quan C G, Kobayashi T and Lee C 2011 Piezoelectric MEMS energy harvester for low-frequency vibrations with wideband operation range and steadily increased output power *J. Microelectromech. Syst.* **20** 1131–42
[5] Shen D N, Park J H, Noh J H, Choe S Y, Kim S H, Wikle H C III and Kim D J 2009 Micromachined PZT cantilever based on SOI structure for low frequency vibration energy harvesting *Sensors Actuators* A **154** 103–8
[6] Liu J Q, Fang H B, Xu Z Y, Mao X H, Shen X C, Chen D, Liao H and Cai B C 2008 A MEMS-based piezoelectric power generator array for vibration energy harvesting *J. Microelectron.* **39** 802–6
[7] Shu Y C and Lien I C 2006 Efficiency of energy conversion for a piezoelectric power harvesting systems *J. Micromech. Microeng.* **16** 2429–38
[8] Marzencki M, Ammar Y and Bastour S 2007 Integrated power harvesting system including a MEMS generator and a power management circuit *Proc. Int. Conf. on Solid-State Sensors, Actuators and Microsystems (Lyon, France)* pp 887–90
[9] Yen T T, Hirasawa T, Wright P K, Pisanao A P and Lin L W 2011 Corrugated aluminum nitride energy harvesters for high energy converstion effectiveness *J. Micromech. Microeng.* **21** 085037
[10] Fang H B, Liu J Q, Xu Z Y, Dong L, Wang L, Chen D, Cai B C and Liu Y 2006 Fabrication and performance of MEMS-based piezoelectric power generator for vibration energy harvesting *J. Microelectron.* **37** 1280–4
[11] Shen D N, Park J H, Ajitsaria J, Choe S Y, Wikle H C III and Kim D J 2008 The design, fabrication and evaluation of a MEMS PZT cantilever with an integrated Si proof mass for vibration energy harvesting *J. Micromech. Microeng.* **18** 055017
[12] Jeon Y B, Sood R, Jeong J H and Kim S G 2005 MEMS power generator with transverse mode thin film PZT *Sensors Actuators* A **122** 16–22
[13] Lei A, Xu R, Thyssen A, Stoot A C, Christiansen T L, Hansen K, Lou-Moller R, Thomesen E V and Birkelund K 2011 MEMS-based thick film PZT vibrational energy harvester *MEMS 2011 (Cancun, MEXICO)* pp 125–8
[14] Lee B S, Lin S C, Wu W J, Wang X Y, Chang P Z and Lee C K 2009 Piezoelectric MEMS generators fabricated with an aerosol deposition PZT thin film *J. Micromech. Microeng.* **19** 065014
[15] Tanaka K, Konishi T, Ide M and Sugiyama S 2006 Wafer bonding of lead zirconate titanate to Si using an intermediate gold layer for microdevice application *J. Micromech. Microeng.* **16** 815–20
[16] Aktakka E E, Peterson R L and Najafi K 2011 Thinned-PZT on SOI process and design optimization for piezoelectric inertial energy harvesting *Transducer's 11 (Beijing, China)* pp 1649–52
[17] Xu X H and Chu J R 2008 Preparation of a high-quality PZT thick film with performance comparable to those of bulk materials for applications in MEMS *J. Micromech. Microeng.* **18** 065001
[18] Wang Z H, Miao J M and Tan C W 2009 Acoustic transducers with a perforated damping backplate based on PZT/silicon wafer bonding technique *Sensors Actuators* A **149** 277–83
[19] Vallin O, Jonsson K and Lindberg U 2005 Adhesion qualification methods for wafer bonding *Mater. Sci. Eng.* R **50** 109–65
[20] Lu F, Lee H P and Lim S P 2004 Modeling and analysis of micro piezoelectric power generators for micro-electromechanical-systems applications *Smart Mater. Struct.* **13** 57–63
[21] Takahashi S, Hirose S and Uchino K 1994 Stability of PZT piezoelectric ceramic under vibration level change *J. Am. Ceram. Soc.* **77** 2429–32
[22] Yao L Q, Zhang J G, Lu L and Lai M O 2004 Nonlinear dynamic characteristics of piezoelectric bending actuators under strong applied electric field *J. Microelctromech. Syst.* **13** 645–52
[23] Tang G, Liu J Q, Liu H S, Li Y G, Yang C S, He D N, DzungDao V, Tanaka K and Sugiyama S 2011 Piezoelectric MEMS generator based on the bulk PZT/Silicon wafer bonding technique *Phys. Status Solidi* A **208** 2913–9
[24] Ramsay M J and Clark W W 2001 Piezoelectric energy harvesting for BioMEMS applications *Proc. SPIE* **4332** 429–38
[25] Roundy S, Paul K W and Jan R 2003 A study of low level vibrations as a power source for wireless sensor nodes *Comput. Commun.* **26** 1131–44